CO Gas Kinematics & Excitation in a filamentary IRDC

I. Jiménez-Serra[1], P. Caselli[2], F. Fontani[3], J.C. Tan[4], J.D. Henshaw[2], J. Kainulainen[5] & A. K. Hernandez[6]

[1] European Southern Observatory (Germany) [2] University of Leeds (UK) [3] Osservatorio Astrofisico di Arcetri (Italy) [4] University of Florida (USA)
[5] Max-Planck-Institute for Astronomy (Germany) [6] University of Wisconsin-Madison (USA)

Theories of cloud formation propose that molecular clouds form in highly dynamical environments by the interaction of converging gas flows or cloud-cloud collisions. The determination of the dynamics and physical conditions of the molecular gas in clouds at the early stages of their evolution is thus essential to establish the dynamical imprints of such collisions, and to infer the physical processes involved in their formation. We present large-scale (1.7 pc×3.4 pc) multi-transition ^{13}CO and C^{18}O J=1→0, J=2→1 and J=3→2 OTF-maps toward the IRDC G035.39-00.33. This cloud shows a very filamentary structure and relatively little star formation activity, suggestive of its youth, and where evidence for a flow-flow collision has recently been reported [1]. Our study reveals that the CO gas is distributed in three different molecular filaments, where their motions are characterized by a north-south velocity gradient of 0.4-0.8 kms^{-1}pc^{-1}. Several scenarios are proposed to explain the peculiar kinematic structure detected in G035.39-00.33.

a) Morphology of the CO filaments in G035.39-00.33

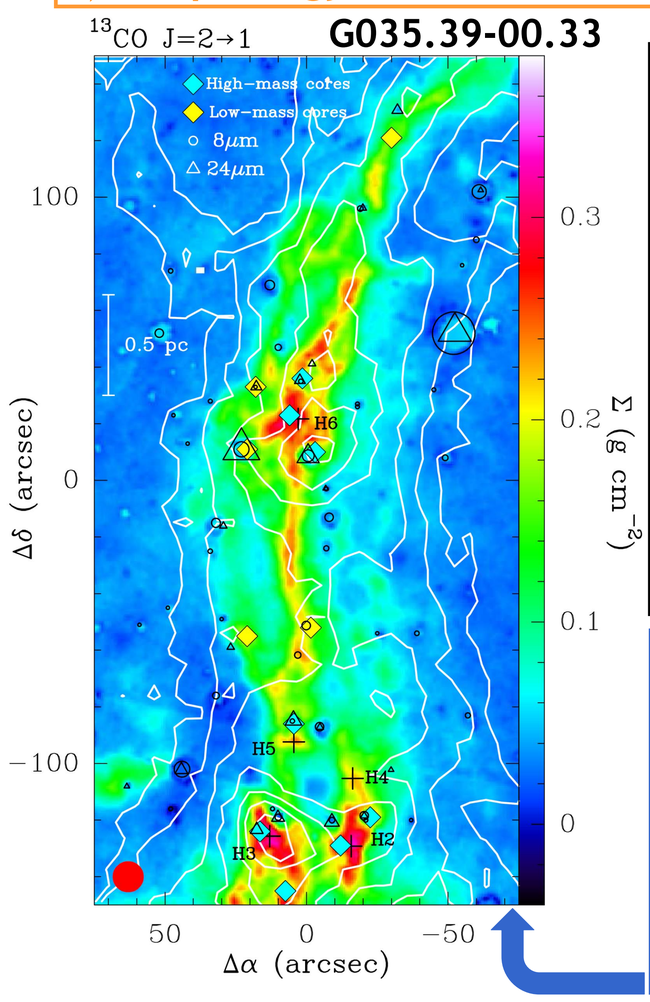

- CO follows the mass surface density map in G035.39-00.33 (Fig.1).
- CO is distributed in three different filaments (F1, F2 & F3; Fig.2).
- F1, F2 & F3 are separated in velocity space by ~3 kms^{-1} (see also [2]).
- Massive cores are found at the intersecting regions between F1 and F2/F3 (Figs.1 & 2).
- F1 and F2/F3 may be interacting.

Fig.1.- Integrated intensity image of ^{13}CO(2→1) measured with the IRAM 30m telescope for the velocity range between 40 and 50 kms^{-1} (white contours), and superimposed on the mass surface density map of [3] (in colour). Crosses indicate the location of the massive cores in the cloud [4]. Black open circles and black open triangles show, respectively, the 8μm and 24μm sources detected with *Spitzer* [1]; and yellow and light-blue filled diamonds show the low-mass and high-mass cores found with *Herschel* [5]. Beam size of the IRAM 30m observations is ~11".

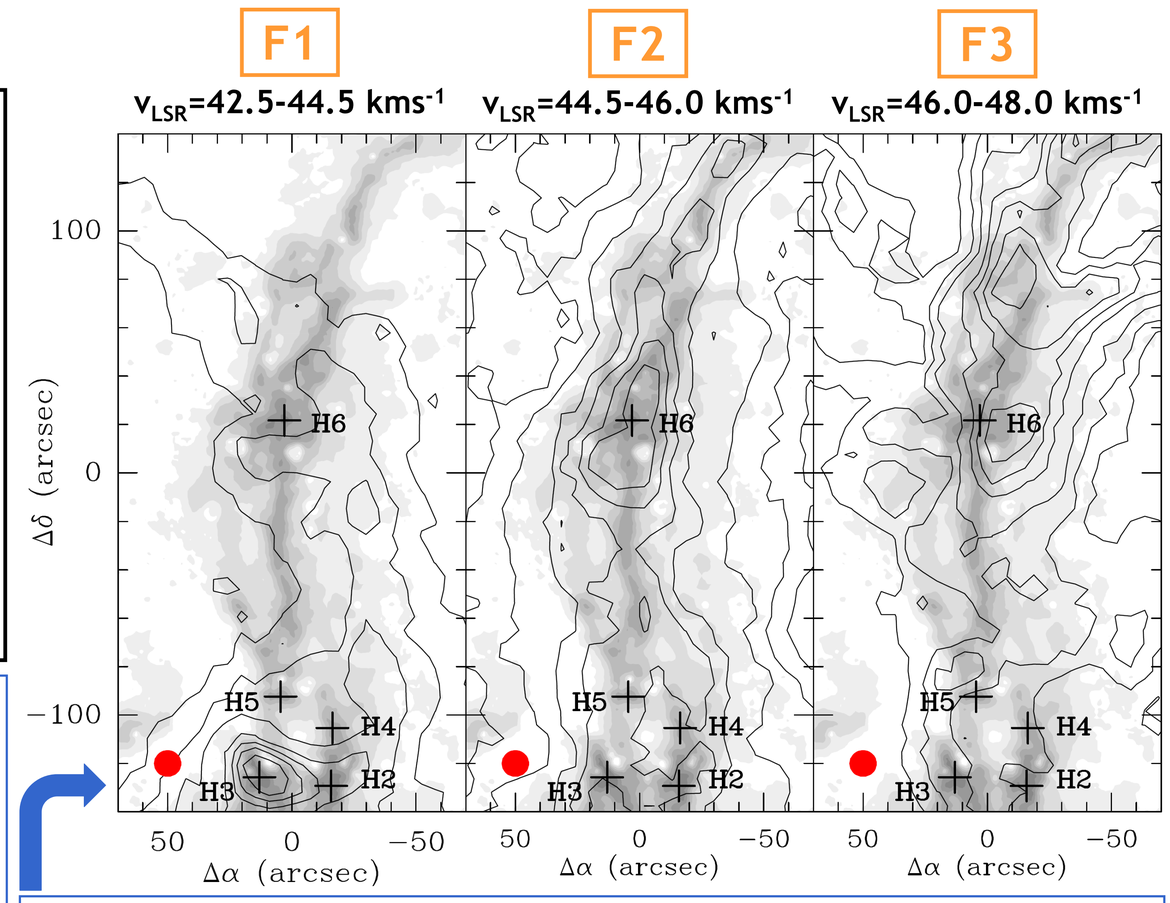

Fig.2.- Integrated intensity maps of the ^{13}CO(2→1) filaments (F1, F2 & F3) detected toward G035.39-00.33. These maps are superimposed on the mass surface density map of [3] (grey scale). Crosses show the location of the massive cores detected in the cloud [4]. Massive cores are found at the intersecting regions between filaments F1 and F2/F3.

b) Kinematics of the individual filaments F1, F2 & F3

Multi-Gaussian profile fits to the ^{13}CO and C^{18}O lines

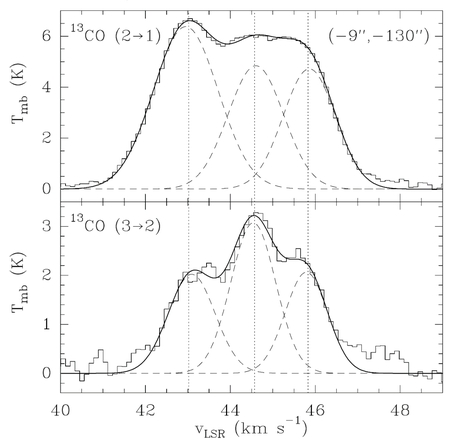

Fig.3.- Example of multi-Gaussian profile fitting to the ^{13}CO(2→1) and ^{13}CO(3→2) lines.

Distribution of v_{LSR} and Δv for every filament (Figs.4 & 5).

- Smooth north-south velocity gradient in F1, F2 & F3 (Fig.4).
- ^{13}CO and C^{18}O supersonic motions. Lines become broader toward the IRDC edges (Fig. 5).
- Real increase of σ_{NT} in the low-density gas.

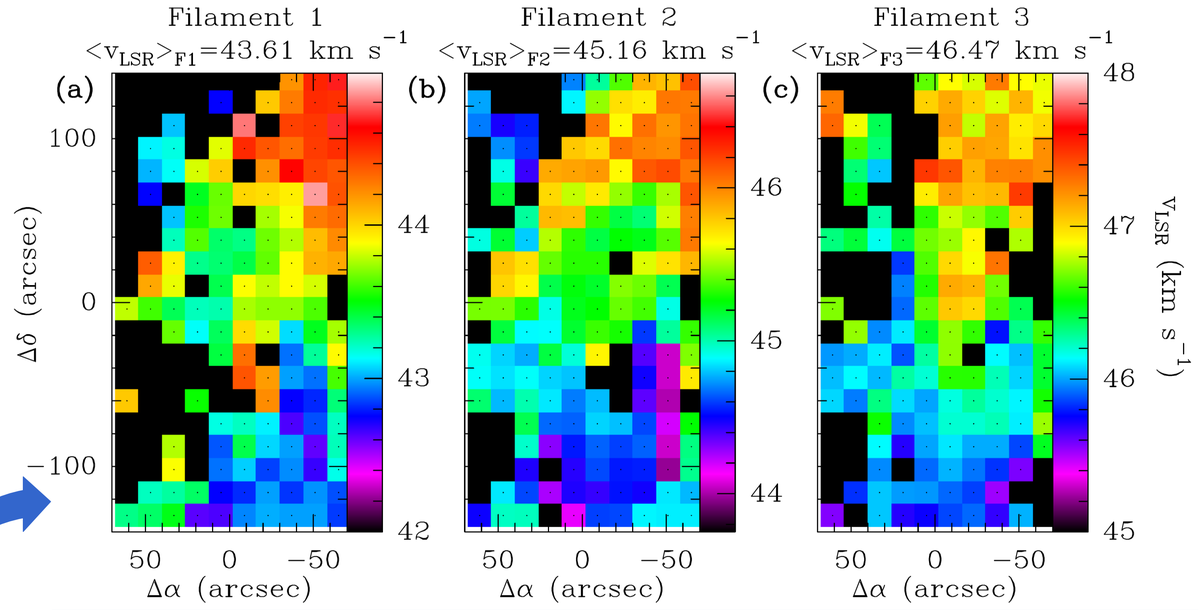

Fig.4 Spatial distribution of v_{LSR} derived from ^{13}CO(2→1) for filaments F1, F2 & F3 by using our multi-Gaussian fitting procedure. The velocity range (color scale on the right) varies from panel to panel. The average v_{LSR} for every filament is shown in the upper part of every panel. A smooth north-south velocity gradient of ~0.4-0.8 kms^{-1}pc^{-1} is detected in all filaments.

c) Physical properties of the CO gas in F1, F2 & F3

LVG modelling of the ^{13}CO lines → $n(H_2)$, $N(^{13}CO)$, Tex, τ

Average physical properties of filaments F1, F2 & F3 derived from ^{13}CO.

Filament	T_{kin} (K)	$n(H_2)$ (cm^{-3})	$N(^{13}CO)$ (cm^{-2})	$T_{ex}(2\rightarrow1)$ (K)	$T_{ex}(3\rightarrow2)$ (K)	τ_{21}	τ_{32}	$\Sigma_{^{13}CO}$ (g cm^{-2})	Mass ($M_\odot$)
1	15	5100	9.4×10^{15}	9.7	7.8	2.0	1.3	0.012	4300
2	15	7500	1.4×10^{16}	11.0	8.9	2.7	2.0	0.020	15000
3	15	7300	9.6×10^{15}	10.7	8.6	2.2	1.5	0.012	10800
1	17	4000	8.2×10^{15}	9.9	7.9	1.8	1.1	0.010	3800
2	17	5600	1.3×10^{16}	11.3	9.0	2.5	2.0	0.016	14500
3	17	5500	8.9×10^{15}	10.9	8.7	2.0	1.4	0.011	9900

Filaments F2 & F3 more dense and more massive than F1!

Fig.5.- Non-termal velocity dispersion, σ_{NT}, derived from ^{13}CO(2→1), ^{13}CO(3→2) and C^{18}O(2→1), as a function of T_{mb} for filaments F1, F2 & F3. Dotted line is the sound speed (c_s=0.25 kms^{-1}). Solid red lines are the fit to the data in the form $\sigma_{NT}=a_x(T_{mb})^b$, and green dashed lines show the average non-termal dispersion in every filament. Gas motions are supersonic and lines become broader at the IRDC edges. Real increase of turbulence in the low-density gas.

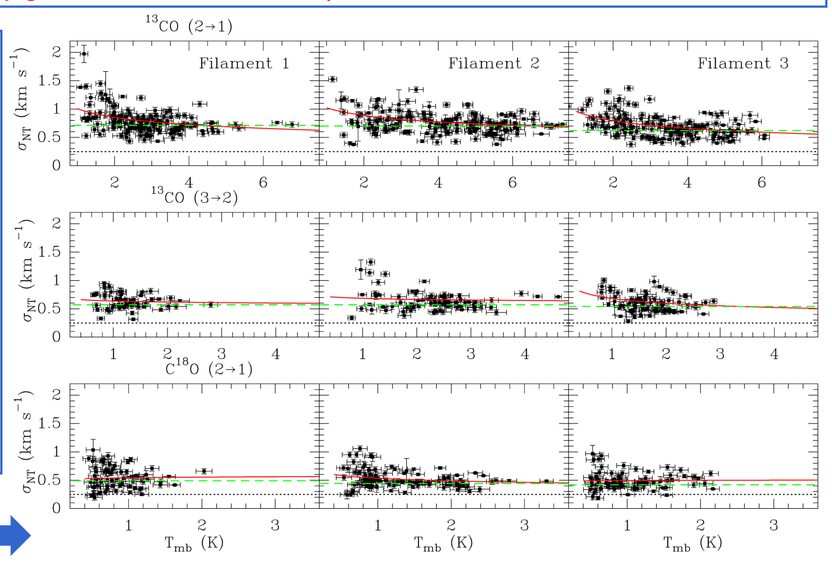

Origin of the velocity gradient in G035.39-00.33.- Several scenarios are proposed: i) rotation [6]; ii) gas accretion flows onto the massive core H6 (accretion rate ~4700 M_o Myr^{-1}), in a similar fashion to those reported toward high-mass and low-mass star forming regions [7,8]; or iii) large-scale turbulence with a steep turbulence power spectrum [9]. The increase of σ_{NT} in the low-density gas could be produced by dissipasion of turbulence and energy at the dense interface of the cloud-cloud collision, which may have induced the formation of the IRDC [1,2].

[1] Jimenez-Serra et al. (2010), MNRAS, 406, 187
[2] Henshaw et al. (2013), MNRAS, 428, 3425
[3] Kainulainen & Tan (2013), A&A, 549A, 53K
[4] Butler & Tan (2012), ApJ, 467, 207
[5] Nguyen Luong et al. (2011), A&A, 535, 76
[6] Ragan et al. (2012), ApJ, 746, 174
[7] Galvan-Madrid et al. (2009), ApJ, 706, 1036
[8] Kirk et al. (2013), ApJ, 766, 115
[9] Burkert & Bodenheimer (2000), ApJ, 543, 822